In target yields for EURISOL RIB production

D. Ene[1,2], S. Chabod[1], J. C. David[1], D. Doré[1], D. Ridikas[1]

[1]CEA-Saclay, IRFU / Service de Physique Nucléaire, 91191 Gif-sur-Yvette
[2]"Horia Hulubei" National Institute for Physics and Nuclear Engineering, P.O. Box MG-6, 76900 Bucharest, Romania

Abstract:

The goal of this paper is the estimation of the neutron-induced fission fragment productions using the most recent optimized design of the EURISOL converter-fission target assembly. Calculation of the fission yields has been done using evaluated yields for the fission products tabulated at three energies of the neutron field. This approach was checked by an alternative method that uses CINDER to determine fission production rates. In-target fission yields were further derived and discussed for six isotopes of interest and six fission target configurations. The report provides detailed fission yields distributions for selected relevant nuclides and discuses the potential of the investigated target material configurations to enhance the production of specific nuclear species.

A comparative study between the two production scenarios used in the design, converter and direct methods, in terms of neutron and fission rate distributions and relevant fission product yields is finally carried-out. The results clearly confirm that the two production systems are complementary allowing at the same time to have a picture of the figure of merit of the future facility.

1. Introduction

EURISOL, (see www.eurisol.org) is the conceptual design of a facility for the production of high intensity secondary beams based on the ISOL method developed in the frame of a large European collaboration. In the design the primary proton driver (1GeV, 4mA) has multi-deliver beams allowing various production modes. In so called "converter method" the radioactive ion beams (RIBs) are produced by secondary low energy neutrons from a liquid Hg converter target by inducing fissions in a UCx targets. For this two stage target assembly the aimed fission rates (10^{15} fissions s^{-1}) is achieved by using ^{235}U fissile target material that at the excitation energy of the incoming neutrons (in average ~100 keV) has the optimal production. Within this scenario high intensity very neutron rich yields are produced concentrated in a relatively narrow area of the nuclide chart. Higher excitation products that populate much broader range on the nuclide chart are obtained additionally by direct interaction of the proton beam with various target materials. After extraction, ionisation and selection the RIB will be re-accelerated. The designed linear post accelerator will allow acceleration of $^{132}Sn^{25+}$ the reference case of the facility at the energy up to 150MeV u^{-1} and intensity of ~10^{13} pps.

Within EURISOL task #11 "Beam Intensity Calculations" the in-target production rate calculations for the direct method see (Chabod, 2008) with the Monte Carlo code MCNPX (Hendricks, 2005) coupled with CINDER (Wilson and England, 2001) for 0.1 mA proton beam of 1 GeV energy on the target have been performed.

The goal of this technical report was the estimation of the neutron-induced fission fragment productions using the most recent designed performances of the converter-fission target assembly. Previous analyses were carried-out to demonstrate technical feasibility of the converter-fission target assembly. Since one of the most important design criteria for the EURISOL facility are the production rates of the nuclides relevant for experiment it is very important to assess and compare with other potential production scenarios the fission fragment production of the optimized two stage target configuration.

In this context the methodology has been developed to estimate the in-target production rates using evaluated tabular yields for the fission products. The developed approach was also validated by an alternative method that uses CINDER to determine fission production rates.

Based on this method the in-target fission yields were further derived and discussed for six isotopes of interest and six fission target configurations.

The study ends up with a comparative study between the two production scenarios used in the design, converter and direct methods. The neutron and fission rate distributions as well as the relevant fission product yields derived in both cases for actinide based targets were analysed and discussed.

2. Calculation method

2.1. *Calculated quantities*

The calculation method used is based on two steps as follows.

I. Determination of the fission rate in the spallation neutron field

$$FR = N_i \left(\int_0^{20MeV} \sigma f(E)\Phi(E)dE + \sigma f(20MeV) \int_{20MeV}^{1GeV} \Phi(E)dE \right) \quad (1)$$

At energies higher than 20 MeV MCNPX code uses a constant fission cross section value to calculate the neutron induced fission rates. This value corresponds to the neutron energy of 20 MeV, see www.nndc.bnl.gov. In order to check the validity of this approximation we have calculated fission cross sections using XSEX3 code from LCS-code system (Prael et al., 1989) from the MCNPX package. The check was done for few incident energy values as given in the Table 1.

Table 1 Fission cross section (barn) comparison.

Energy (MeV)	^{232}Th		^{238}U	
	MCNPX	XSEX3	MCNPX	XSEX3
100	0.62	0.625	1.46	1.463
200	0.62	0.904	1.46	1.474
500	0.62	1.007	1.46	1.467
1000	0.62	0.937	1.46	1.293

One can see that if for ^{238}U it was found a quite good agreement for ^{232}Th the difference reaches a factor of about 40%. Nevertheless the effect of these differences is negligible upon the fission rates obtained in this work since (see chapter. 3.1.2) the neutron high energy distribution is not important.

II. Calculation of the fission yields

Individual nuclide production yields in direct reactions have been determined using MCNPX followed by the evolution code CINDER calculations, see (Chabod, 2008).

In this work, an alternative approach based on recommended tabular yields for the fission products given in (England and Rider, 1994) has been chosen for production targets of the converter target assembly. These recommended yields are tabulated at several energies: thermal energies (T), fission spectrum energies (F), 14 MeV High Energy (H).

$$Yield = T\int_{0}^{ET}\sigma_f(E)\Phi(E)dE + F\int_{ET}^{EF}\sigma_f(E)\Phi(E)dE + H\int_{EF}^{1GeV}\sigma_f(E)\Phi(E)dE \quad (2)$$

where:
T = fission yield for thermal energy (0.0253eV),
F = fission yield for fast energy (2 MeV),
H = fission yield for high energy (14 MeV)
while the integral limits were chosen as follow:
ET = 5 keV
EF = 5 MeV

Only for verification purposes individual nuclide production yields in fission reactions were determined also using MCNPX followed by CINDER code procedure. See discussion inside the chapter 3.1.3.

Distribution of nuclides produced by fission is concentrated in a relatively narrow area of the nuclide chart. Six isotopes of interest recommended by NUPECC board (Cornell, 2003)) were analysed here: Ni, Ga, Kr, Ag, Sn, Xe. In the analysis six target assemblies configurations were accounted: five cases based on Uranium compounds with ^{235}U percentages of: 99.99, 20, 3, 0.72 (natural Uranium) and 0.02 (depleted Uranium) as well as ^{232}Th material.

An automatic procedure was developed to post process the MCNPX results and to calculate the yields via Eq. 2 producing the total production in the Uranium compounds by the summation of the component nuclide distributions.

2.2. *Model and parameters used in simulations*

The MCNPX2.5.0 variant was used in simulations. The following options were used by the code: i) all particles produced by the incident protons were transported; ii) "CEM2k" that includes intranuclear cascade model (CEM2k) together with a fission-evaporation model; iii) "mix and match" allowing the use of available neutron and proton data tables until their upper energy limits followed further by models; iv) neutron data tables from ENDF/B-VII libraries at 300 K whenever available; v) importance as biasing method. Calculations were run to reach the statistical errors less than 5% for all results. The Figure 1 shows the target set-up as model build by MC code.

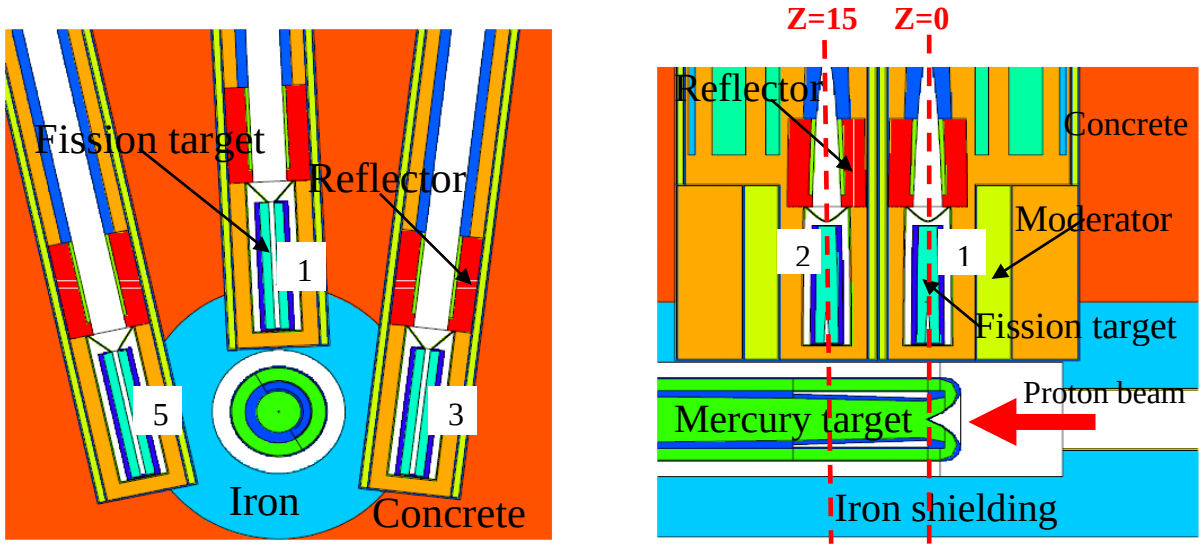

Figure 1: Geometry model used in MCNPX simulations. Left: XY cross section in z=0; Right: YZ cross section.

The geometry model received from the Task# 2 & 4 (Romanets, 2009) represents the last design variant able to accommodate 30 kW load heat. In the model, clusters of three fission targets (see the left panel of the Fig.1) are placed closed to the spallation neutron source as is shown in the right side of the Fig.1 in the following structure: target #5 (T#5), T#1, T#3 at z=0 cm, coordinate scaled on the proton beam axis that corresponds to the beam impact into the converter and respectively T#4, T#2, T#6 at z=15 cm. The production targets are cylinders with internal axial holes, having a volume of 181 cm^3. A homogenized material of fissile-graphite compound with mass rate 1/20 and the actinide mass of 15 g was accounted in all calculations performed. Detailed information about the optimized fission target is given in the chapter 3.2.1 (Table 8). For all configurations studied based on Uranium the moderator material was chosen the water while the reflector material was taken the beryllium oxide. Only in case of Thorium used as fissile the iron was used in the model for both moderator and reflector materials.

3. Results and discussion

The results presented are normalized to 1 mA intensity proton beam on the target to allow easily the desired scaling to other values. The text specifies when the normalisation has been done for 4 MW power beam.

3.1. *In-target fission yields*

3.1.1 Neutron flux

The neutron energy spectrum at the position of fission targets affects the fission rates. The neutron spectrum within fission target is determined by: i) the spallation neutron spectrum; ii) the material present in the moderator/reflector assembly; iii) the uranium fission neutron spectrum; iv) spectrum of neutrons from (n,xn) reactions; v) to some extent by other materials present in the target assembly.

Results of the calculations for the neutron flux are reported in the Fig. 2 and Table 2. The total neutron fluxes for a specific configuration are distributed quite uniformly over the six fission targets that confirm that the neutrons arising from the converter have a nearly isotropic angular distribution. However a slight enhance of the total flux can be noticed for the targets placed at z=15 cm following the development of the cascade.

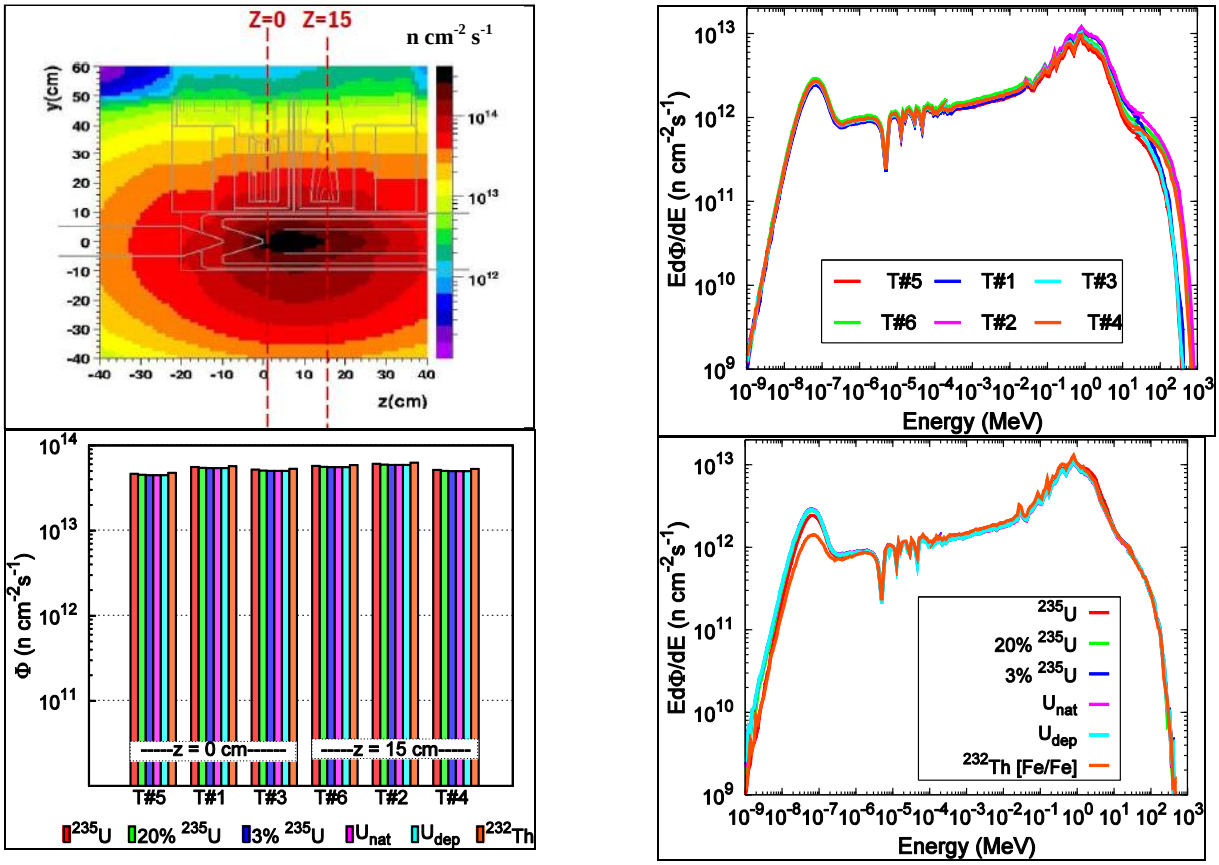

Figure 2: Neutron flux obtained from simulations. On top the ^{235}U configuration is presented with the total flux profile in the midplane of the configuration (right) and energy distribution within the six fission targets (left). Bottom side compares the investigated material configurations: on the right, integrated spectra distributed through the six targets and on left energy dependence of the spectra for the fission target #1 (see Fig.1).

Table 2: Neutron flux [neutrons cm^{-2} s^{-1}] averaged over three fission targets placed at the same level against the proton beam axis for all target assembly configurations.

Configuration	plan z=0 cm	plan z=15 cm
^{235}U	5.1380 10^{13}	5.6604 10^{13}
20% ^{235}U	5.0084 10^{13}	5.5219 10^{13}
3% ^{235}U	4.9764 10^{13}	5.4867 10^{13}
U_{nat}	4.9707 10^{13}	5.4811 10^{13}
U_{dep}	4.9700 10^{13}	5.4794 10^{13}
^{232}Th	5.2496 10^{13}	5.8150 10^{13}

This uniformity is kept for all material configurations under analysis as can be seen in the bottom side of the Fig. 2. As is shown in this figure the neutron flux energy distribution is dominated by the evaporative neutrons with a maximum energy of about 600 keV, having a negligible high energy domain (less than 3 %) and an important thermal component.

3.1.2 Fission rates

Detailed fission rates information was determined from simulations in function of the neutron energy and the integrated spectrum to give a thorough characterisation for the ^{235}U case and for other five material configurations investigated (Eq. 1, Fig.2).

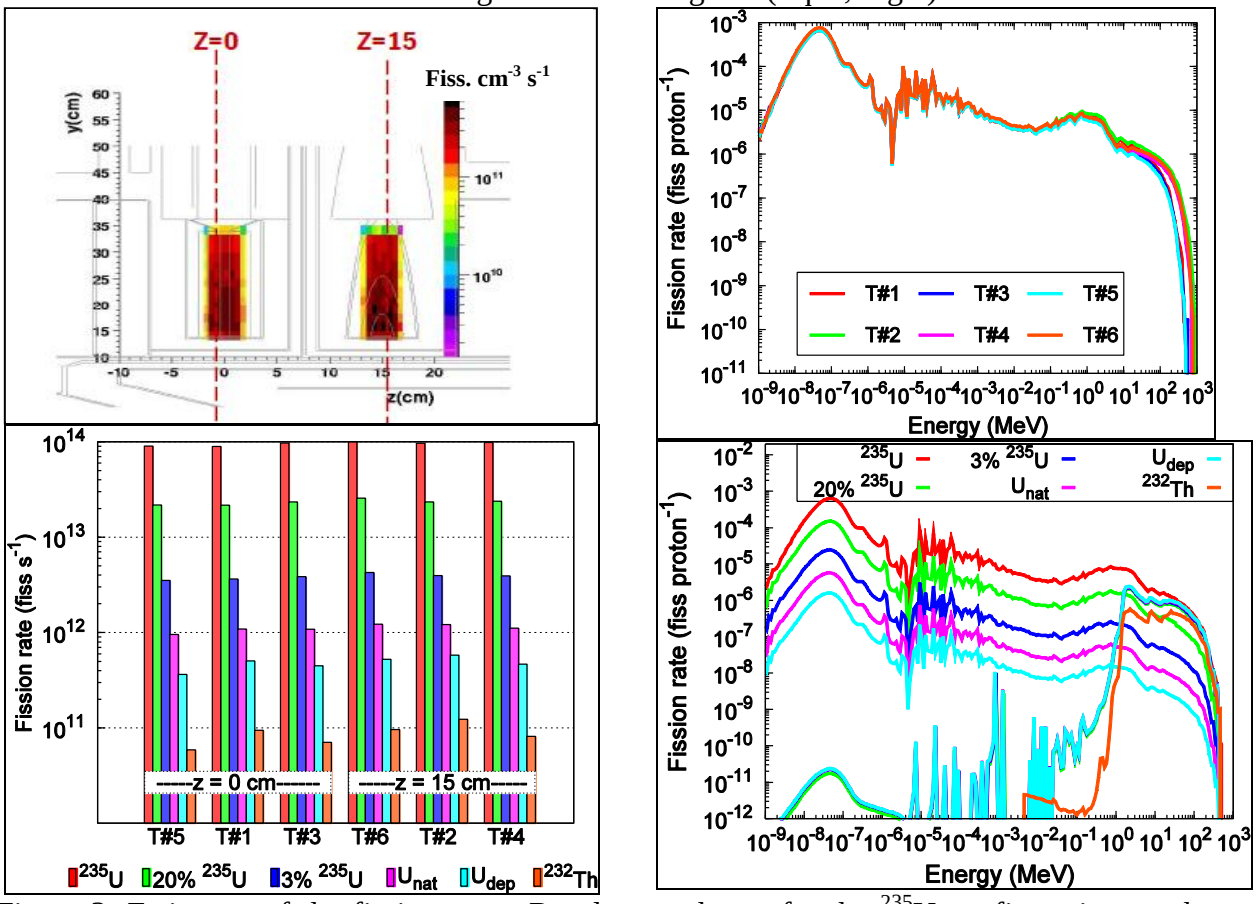

Figure 3: Estimates of the fission rates. Results are shown for the ^{235}U configuration on the top: fission density spatial distribution in the plane x=0 (left) and energy distribution within the six fission targets (right). Bottom: total fission rates in the six targets (left) and distributions vs energy (right) for analyzed material configurations (same color is used for the two components of the compound).

Due to the low neutron energies the fission process is induced essentially in ^{235}U that has high neutron fission cross section for this energy range (see the bottom side of the Fig. 3). This figure shows the decreasing of the fission rates with the reduction of the ^{235}U concentration in the compounds as well as the low level values given by ^{238}U and ^{232}Th.

Consistent with the above discussion the Table 3 shows clearly that for all accounted Uranium compounds more than half of the total fission rates are due to fission of the ^{235}U component.

Table 3: Fission rates for all target assembly configurations [fissions s^{-1} mA^{-1}]. The percentage of the ^{235}U fission rate contribution to the total is also shown.

Configuration	**^{235}U***	**^{238}U**	**Total**	**^{235}U [%]**
^{235}U	$5.7689\ 10^{14}$	-	$5.7689\ 10^{14}$	100
20% ^{235}U	$1.3823\ 10^{14}$	$1.2021\ 10^{12}$	$1.3943\ 10^{14}$	99.14
3% ^{235}U	$2.1712\ 10^{13}$	$1.3931\ 10^{12}$	$2.3106\ 10^{13}$	93.97
U_{nat}	$5.2449\ 10^{12}$	$1.4172\ 10^{12}$	$6.6621\ 10^{12}$	78.73
U_{dep}	$1.4591\ 10^{12}$	$1.4223\ 10^{12}$	$2.8814\ 10^{12}$	50.64
^{232}Th	$5.2366\ 10^{11}$	-	$5.2366\ 10^{11}$	-

∗ ^{232}Th for Th case

The number of fissions (~10^{15}) per second required by the baseline EURISOL project is thus met for the most favourable producing system (^{235}U case). The use of other Uranium compounds or ^{232}Th reduce the magnitude of yields.

3.1.3 Fission yields

Neutron induced nuclear fission splits ^{235}U, ^{238}U or ^{232}Th into two fragments asymmetrically. Masses of the produced fission fragments range from 60 to 160. The majority of the fission products occur in two peaks at masses about 95 and 140. The figures of the Annex 1 display the tabulated fission product yields distributed by mass that have been used in this work. These curves show that the exact yield is dependent on the parent atom, and also on the energy of the initiating neutron. In general the higher the energy of the state that undergoes nuclear fission, the more likely that the two fission products have similar mass. Hence as the neutron energy increases the valley between the two peaks becomes shallower.

Isotopic distributions of the tabulated yields for the six elements being investigated extend over the ranges given in Table.4. As a matter of example the Table 5 shows the fission rates used as normalisation factors (see Eq. 2), in terms of percentage contributions to the total fission rate, used to determine practically the production yields for T#1. As expected (see Fig. 3) the fission rates used to calculate the fission yields of ^{235}U are dominated by the thermal contribution. In case of ^{238}U the fission yields for fast and high energies are weighted almost equally while for ^{232}Th the high energy factor is almost two times larger than that of the fast energy fissions.

Table 4: Determined isotopes of selected elements

Element	Z	A_{min}	A_{max}
Ni	28	66	82
Ga	31	67	87
Kr	36	83	100
Ag	47	104	130
Sn	50	118	138
Xe	54	131	149

Table 5: Contributions (%) to the total fission rate used for normalisation of the fission yields in T#1

Configuration	Isotope	Therm	Fast	High energy
^{235}U	^{235}U	97.48	2.27	0.25
20% ^{235}U	^{235}U	97.99	1.80	0.20
	^{238}U	0.04	49.07	50.89
3% ^{235}U	^{235}U	98.11	1.70	0.19
	^{238}U	0.04	48.18	51.78
U_{nat}	^{235}U	98.12	1.68	0.19
	^{238}U	0.04	48.03	51.94
U_{dep}	^{235}U	98.12	1.68	0.19
	^{238}U	0.04	48.07	51.98
^{232}Th	^{232}Th	-	34.20	65.80

For a better insight into the problem some partial results are also analysed. The Fig. 4 shows the contributions of partial yields to the total production yield calculated using the mentioned above method. Three representative nuclides were chosen for comparison: i) a light nuclide (Ni), ii) Ag that is placed in the dip zone (between Z=42 and Z=48) of the fission yield distributions and iii) one element from the maxima of the yields distribution (in the figure is shown Xe but Kr has similar features). In case of yields produced by fission of ^{235}U (top panel of the Fig. 4) the strong contribution of the T yield over the whole distribution is clearly seen for Xe (or Kr) reflecting the large value of the fission rate normalisation factor. For Ni and Ag the tails of the distributions are dominated by the H yield component.

The ^{238}U parent fission yield distributions (Fig. 4, bottom side) show that H partial distribution is biased towards the neutron-rich wing of the distributions. One can see also that the fission rate normalisation factors (Table 5) have a less influence upon the total production yield showing differences between the F and H tabulated yields. This difference is pronounced for Ni and Ag where the H yield dominates by far the whole distribution. Only for Xe the total distribution is a combination of two distributions with amplitudes almost equally reflecting the ratio of the normalisation factors. The calculated production yields for ^{232}Th follow almost the same trend as ^{238}U modified by the specific normalisations.

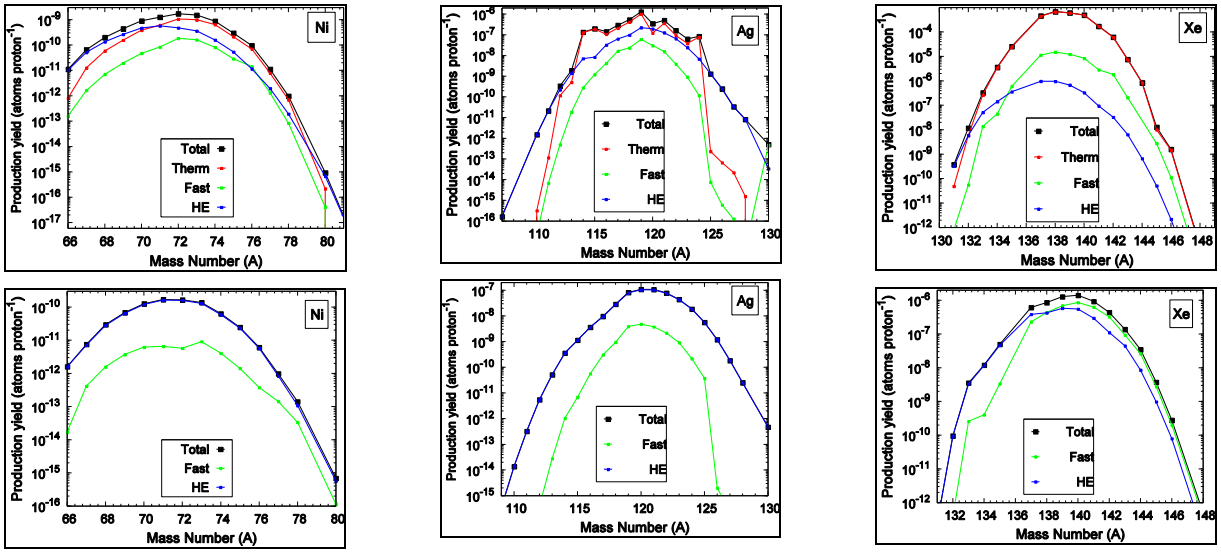

Figure 4: Contribution of partial yields to the production yields of selected isotopes in the target #1configuration based on ^{235}U (top) and Depleted uranium (bottom). From top to bottom the nuclide concerned is ^{235}U and ^{238}U

The total nuclide production of a specific fission product in a uranium compound is given by the superposition of the nuclide distribution of ^{235}U and ^{238}U. The Fig.5 is an illustration of the contributions of these nuclides to the total production yield for natural uranium. All other uranium compounds studied show the same features even though the relative contribution coming from ^{235}U fissions increases with the increasing of ^{235}U percentage in the composition.

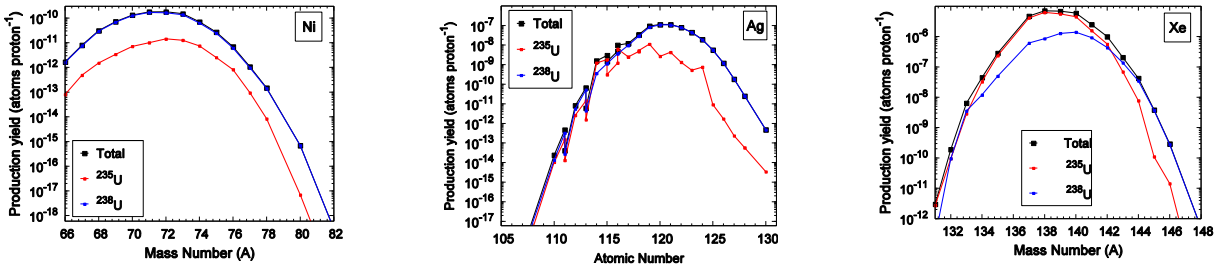

Figure 5: Contribution of the nuclide yields to the production yields of selected isotopes in the target #1configuration based on natural uranium

These curves reveal that the neutron rich side of the total distributions are governed by ^{238}U products. One can see also that light nuclei as Ni, are produced mainly from ^{238}U fissions indicating the influence of higher neutron energy upon the fission fragment distribution of ^{238}U (see Annex 1). Higher energy neutrons reaching the ^{238}U target have an impact also on the number of symmetric fissions populating the elements between Z=42 and Z=48 more strongly. This explains the important contribution of the ^{238}U yield that lasts over a large domain of the Ag isotope distribution. For Kr (Xe) element, placed in the asymmetric fissions region originated from low energy neutrons, the ^{235}U produced partial yield is predominant.

^{238}U is more favourable compared with ^{235}U for producing the most neutron-rich isotopes due to the 3 neutrons difference in the fission nucleus that leads to a neutron excess in the fission fragments of about 1.5 higher. If ^{232}Th is used as target material the neutron excess of the fission fragments is reduced compared with ^{235}U by a factor of about 0.4. Therefore the ^{232}Th nuclide production distribution is shifted towards lighter masses (see Annex 1).

Fig. 6 gives a general view of the yield distributions of the six isotopes under analysis for all studied target configurations.

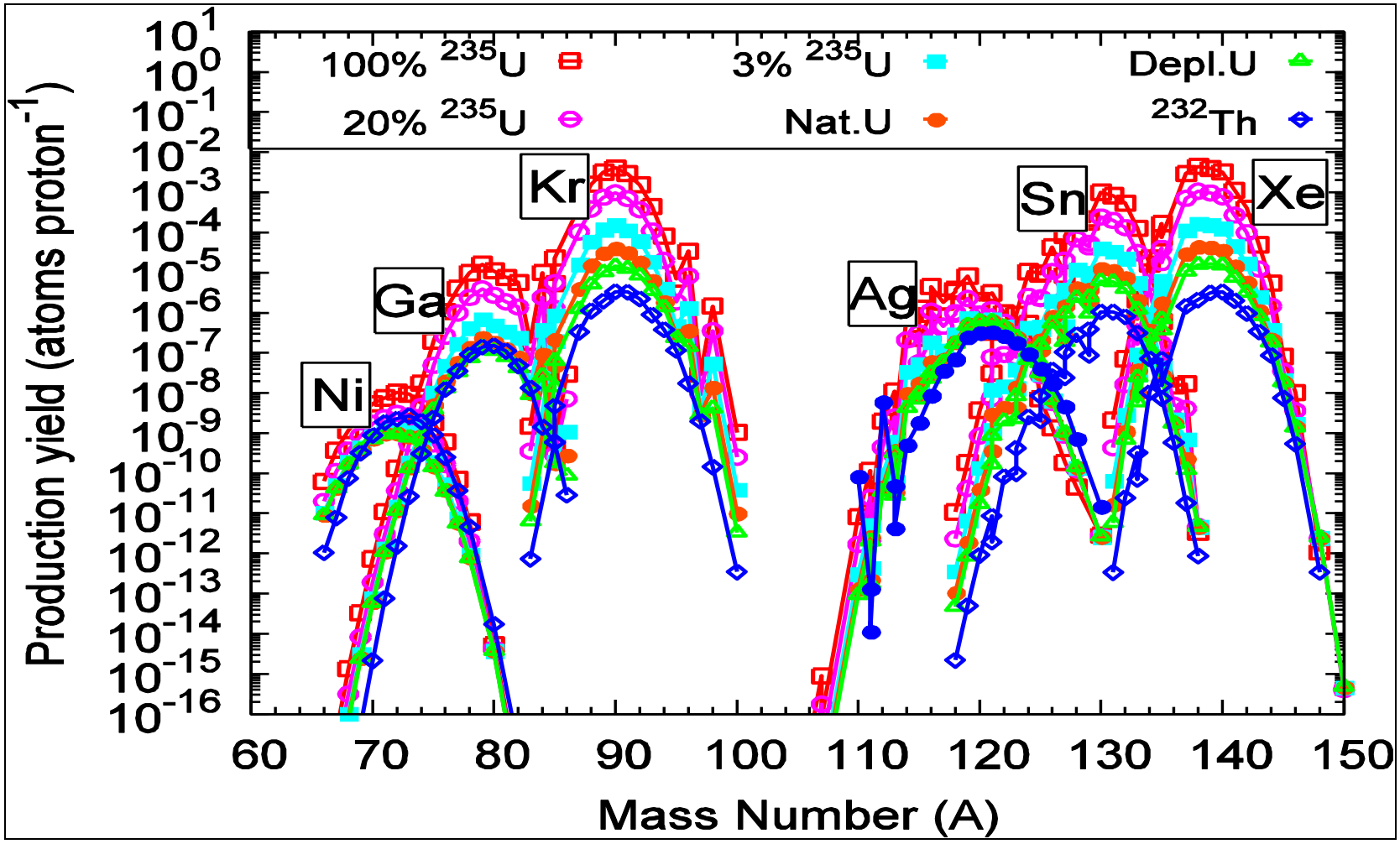

Figure 6: In-target production rates for selected nuclides

Separate graphs of each isotope studied are supplied in the Annex 2. The Annex 3 provides also detailed values of the yields distributions. Note that if in the graphs the yields were drawn accumulating the isomer contributions in the Tables detailed values are presented.

In agreement with the Annex 1 the resulted fission yield isotopic distributions exhibit quite high values for Xe and Kr as well as Sn, which are on the maxima of the distribution, less higher values for Ga and Ag and low values for Ni. For elements produced with high probability (on the fission humps) the differences in the yields between the six configuration systems follow the fission rate trend previously discussed. On the neutron rich side these differences decrease progressively (see the fission rates distributions of the ^{238}U in the Fig. 3 top right) showing that for these elements (neutron rich isotopes) the performances of the analysed Uranium targets become increasingly similarly. As discussed before the ^{238}U component in the compound or the use of ^{232}Th target might extend the yield magnitude over a larger area of interests. For instant, the enhanced production yield above A = 71 for Ni produced from ^{232}Th that reach values even higher than those obtained for 20% ^{235}U configuration in the range (72 < A < 78). It is also visible that higher yields of Ag are produced from ^{232}Th as well ^{238}U over a range beyond A = 125.

The Table 6 summarises the production rates for some isotopes that are most relevant for the experiment (Cornell, 2003).

Table 6: Production yields (atoms s^{-1} mA^{-1}) for several relevant isotopes in the six target configurations analysed

Isotope	^{235}U	20% ^{235}U	3% ^{235}U	U_{nat}	U_{dep}	^{232}Th
^{72}Ni	6.576 10^{7}	1.943 10^{7}	7.836 10^{6}	6.220 10^{6}	5.844 10^{6}	1.4211 10^{7}
^{81}Ga	4.744 10^{10}	1.165 10^{10}	2.136 10^{9}	7.910 10^{8}	4.815 10^{8}	6.973 10^{8}
^{92}Kr	9.530 10^{12}	2.309 10^{12}	3.867 10^{11}	1.148 10^{11}	5.232 10^{10}	1.387 10^{10}
^{126}Ag	8.552 10^{6}	3.611 10^{7}	4.107 10^{7}	4.174 10^{7}	4.185 10^{7}	*1.098 10^{8}*
^{132}Sn	3.372 10^{12}	8.236 10^{11}	1.429 10^{11}	4.663 10^{10}	2.449 10^{10}	4.995 10^{9}
^{142}Xe	2.511 10^{12}	6.125 10^{11}	1.075 10^{11}	3.610 10^{10}	1.969 10^{10}	6.011 10^{9}

In the Fig. 7 a comparison with the SPIRAL2 production yields predictions (by courtesy of M. Fadil) using the method described in (M. Fadil, 2008) for 10^{14} fiss s^{-1} is exhibited for two selected nuclides.

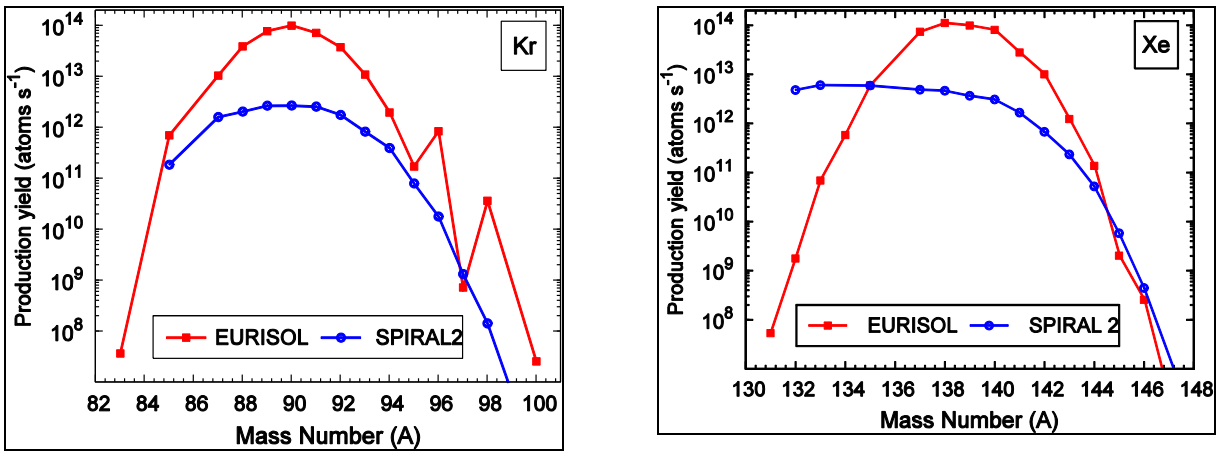

Figure 7: Comparison of the production rates for Kr and Xe estimated for SPIRAL2 (10^{14} fiss s^{-1}) and EURISOL results obtained for ^{235}U target material at 4 mA.

The production rates have been calculated also by means CINDER method (see chapter 2).

For ^{235}U based case where only CINDER thermal fission library is necessary, the direct comparison of the two methods used has lead to a good agreement (see Fig. 8). While for compound materials the combination of both fast and high energy fission yield CINDER libraries (see Table 5) have to be used to get a good agreement especially when the symmetric fissions region is concerned.

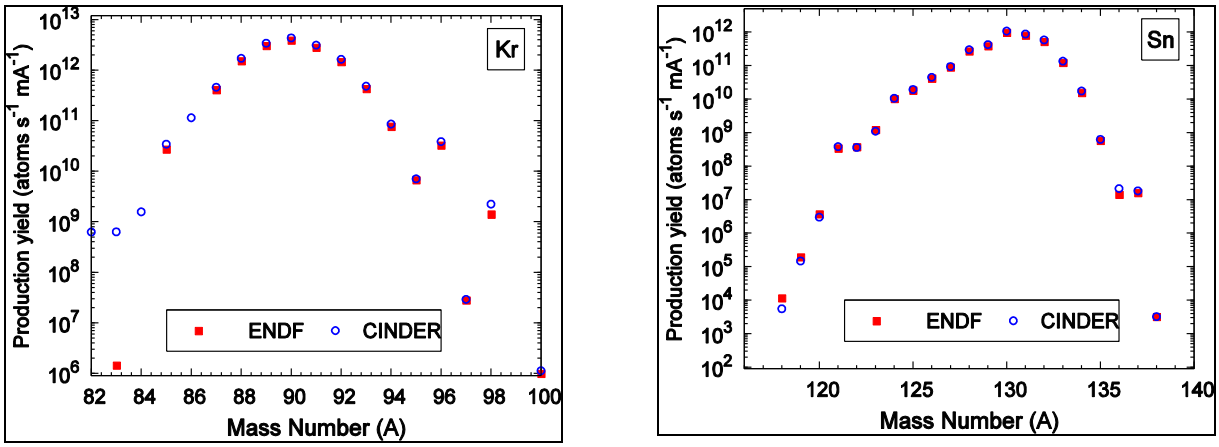

Figure 8: Production rates for Kr and Sn calculated using ENDF fission yields and by CINDER method using code thermal fission library for ^{235}U based target #1

Fig.9 presents the isotopic distributions of the fission products for the six target configurations under comparison. Note that the curve against mass number is smooth. Because of the stability of nuclei with even numbers of protons and/or neutrons, the curve of yield against element tends rather to alternate.

The production distributions are concentrated on very neutron–rich isotopes of a few elements ($32 < Z < 60$) peaked around Xe (Z=54) and Sr (Z = 38). Elements inside the dip of the distribution between Z= 42 and Z=48 are less produced. In case of the uranium compound and ^{232}Th one can see that the gap close to symmetric fission around Z=45 is filled up and that the elements of the tails below Z=30 and above Z=60 are more populated. The mass distribution of the fission products arising from ^{232}Th target is shifted to lighter masses. These features corroborate the conclusions previous discussed regarding the nuclide production contribution of ^{238}U and ^{232}Th results.

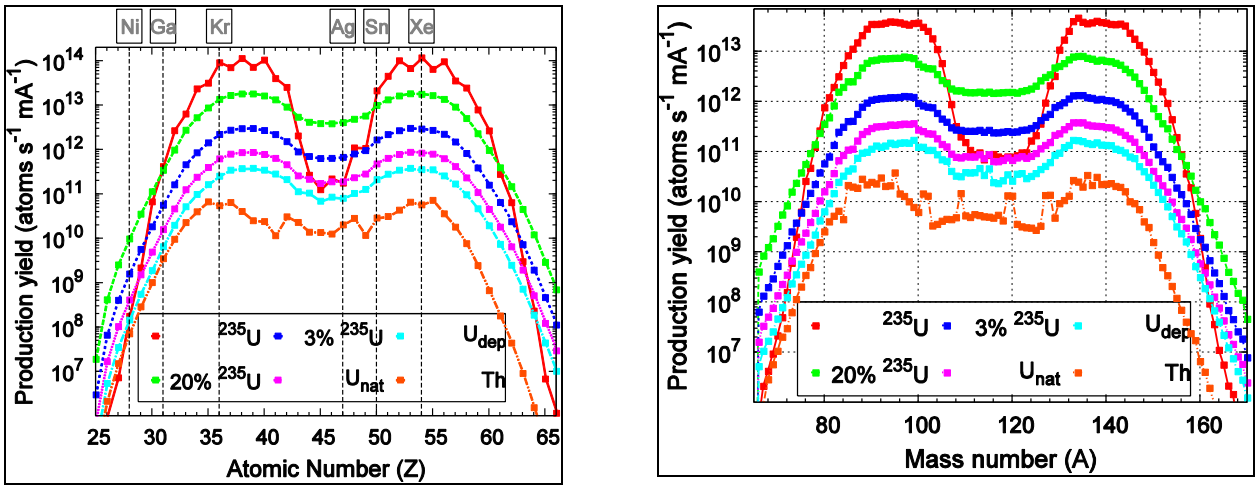

Figure 9: Fission yields in the six accounted configurations as a function of the atomic number Z (left), and the mass number A (right).

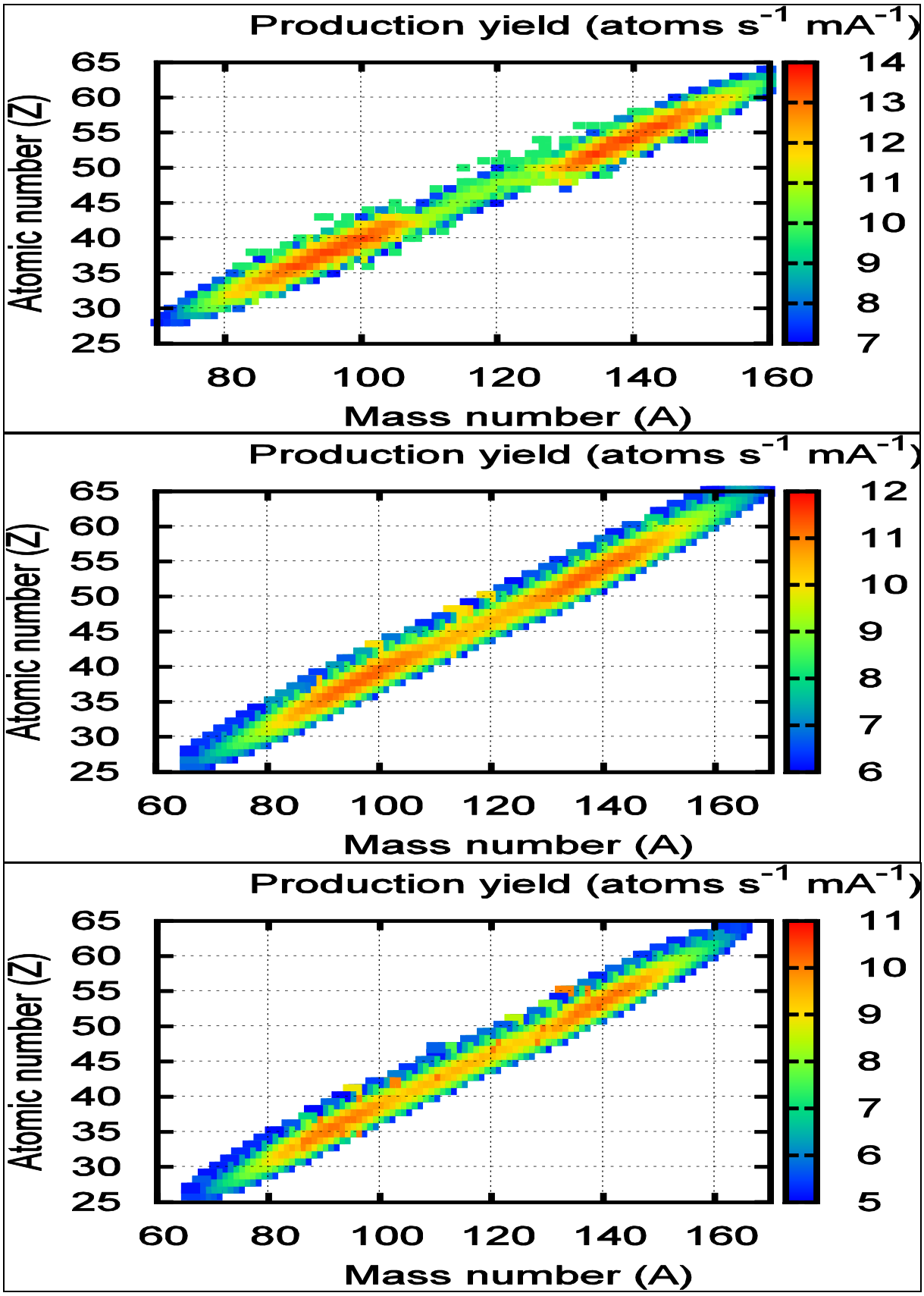

Figure 10: Fission fragment distribution for three of the cases studied: ^{235}U (top), natural uranium (middle), ^{232}Th (down)

Fig. 10 shows the complete fission fragment distributions for three selected target materials.

These maps estimate the distribution and the magnitude for specific fission fragments produced in the targets. In agreement with the above discussions, the largest yields difference between the target materials occurs in the symmetric fission zone induced by fast neutrons (central part of the colour plot).

3.2. *Comparison of the methods*

Besides the converter method an alternative way of producing RIBs, planned in the frame the EURISOL project, is based on direct interactions of high energy protons with target materials. Through the direct interactions are produced mostly the spallation-evaporation and spallation-fission residues. The main nuclide production by spallation-evaporation tends towards proton rich side, while spallation-fission favours neutron-rich isotopes.

Contrary to the method used for the converter target assembly where the in-target production distributions were derived for the optimized designed targets (aiming 10^{15} fissions s^{-1}) the direct target configurations were optimized to obtain maximum production of selected nuclei. In this context a complex study, see (Chabod, 2008) has been developed to estimate and optimize the nuclei production rates for different direct target configurations by varying parameters as: material and volume of the target, or the incident proton energies.

The comparison of the two production systems allows to validate quantitatively the performances of each of the method used, giving also a picture of the figure of merit of the EURISOL facility. In this report it will be analysed and discussed only the actinide targets case.

3.2.1 Input parameters

The Tables 7 and 8 summarize the beam and target characteristics for both methods used in the EURISOL design considered here for the comparison. For direct case (see Table 7) the solid UC_3 target (see the first line of the Table 8) has been optimized in (Chabod, 2008) for

Table 7: Projectile-target combinations optimised within the design studies that are used in the comparison

Method	Primary	Beam energy (GeV)	Beam current (mA)	In target power (kW)	Target material
Direct	p	1	0.1	100	solid UC_3
Converter	p	1	1	30 (4000 on Hg converter)	liquid Hg+UC_x

Table 8: Target parameters for the production of the fission yields by fission/spallation reactions. (In connection with the Table 7)

Method	Density (g cm^{-3})	Target volume (cm^3)	U mass (g)	Geometry
Direct	2.42	407	855 g U_{nat}	cylinder: R=1.8 cm, L=40 cm
Converter	1.88	181	15 g* ^{235}U	ring: R_{ext}=1.75 cm, R_{int}=0.4 cm, L=20 cm

* 90 g total ^{235}U mass from the six designed fission targets.

the production of specific elements like: Be, Ni, Ga, Kr, Sn, Fr. The converter target assembly was optimised through many dedicated neutronics and termohydraulics studies (see Task#2 and 4 on www.eurisol.org) to produced highest fission yields defined by 10^{15} fissions s^{-1} (see Fig.2).

3.2.2 Results

The Table 9 presents comparatively the estimates of the integrated neutron fluxes and the total fission rates for the two compared production scenarios. On the left side of the table one can see that the total neutron flux in the fission target T#1 belonging to the converter target assembly is by more than a factor two larger than the total flux of the secondary neutrons produced in the analysed direct target. The right side of the Table 9 shows almost the same enhancement ratio between the total fission rates.

Table 9: Comparison of the integrated neutron fluxes (left) and of the total fission rates (right) estimated for both methods. Note that for the converter method the results refer to the production target T#1 (see Fig. 2).

Method	**$\Phi_{target\#1}$ (n cm^{-2} s^{-1})**	**Φ_{total} (n cm^{-2} s^{-1})**
Direct		2.473 10^{13}
Converter	5.573 10^{13}	

Method	**^{235}U (fissions s^{-1})**	**^{238}U (fissions s^{-1})**	**Total (fissions s^{-1})**
Direct	1.591 10^{11}	4.042 10^{13}	4.057 10^{13}
Converter	8.926 10^{13}		8.926 10^{13}

The Fig. 11 compares the neutron flux and fission rate distributions versus energy for the two design options. Even though in both cases the neutrons are secondary particles produced by the spallation process, the energy spectra depicted in the left side of this figure show important differences. This can be understood as follows.

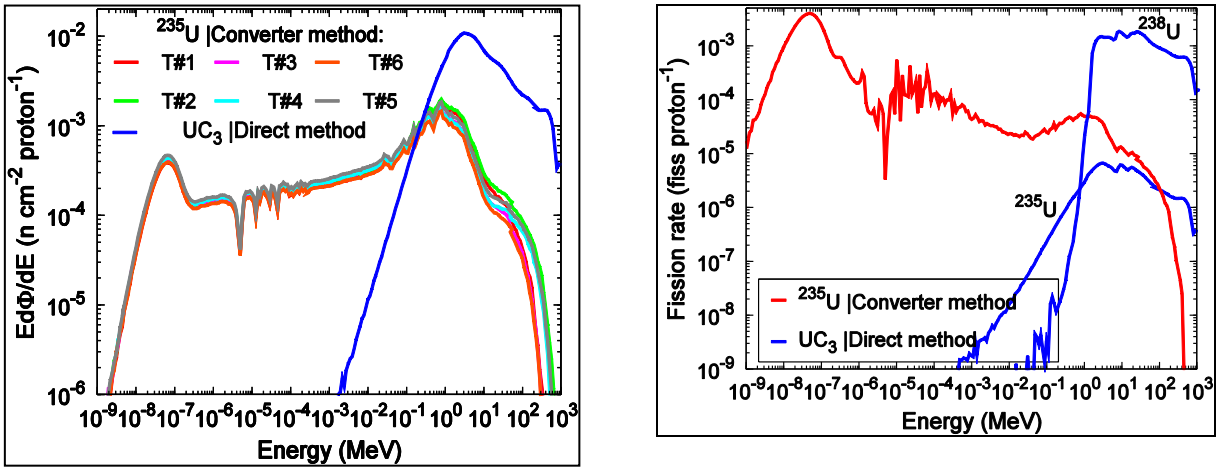

Figure11: Comparison of the resulted energy distribution of the neutron flux (left) and of the fission rate (right). In case of the fission rate distributions the red curve stands for the production target T#1 (see Fig.2)

The charged particle induced cascade might be divided qualitatively into two physical steps: i) a spallation driven high energy phase and ii) a neutron driven evaporation/fission dominated regime. Fast neutrons from the first phase represent the source for the second phase, in which they are loosing energy by collisions and are multiplied by (n, xn) reactions and/or fissions. Depending of the requirement, one has to optimize the target configuration (material, geometry) in conjunction with the primary beam characteristics to enable dominantly one of these physical stages.

As discussed before (chap. 3.1.1) the neutron energy spectrum exiting the Hg converter was optimised (Herrera-Martinez, 2006) to produce the aimed fission rates (~10^{15} fissions s^{-1}). The isotope production rates are proportionally to the fission rates but are also affected by the neutron energy distribution. The optimised converter-fission system is defined by a neutron

average excitation energy of about 100 keV, (62 keV for T#5 to 140 keV for T#2) value derived from the results depicted in the Fig. 11, left side.

For the direct target the neutrons originating from the primary proton reactions have a fast spectrum, that peaks at around 3 MeV and drops drastically at few keV. This energetic neutron distribution (average kinetic energy of around 31 MeV) shows that the moderator effect of the graphite constituent of the production target is less effective (small scattering cross sections at high energy). Consequently, the fission of ^{235}U is negligible (less than 0.5%) compared with that of the ^{238}U, see left panel of the Fig. 9.

The calculated in-target fission yield distributions are presented in the Fig.12 for both scenarios. Note the different normalisations (see Table 7) and the use of the six fission targets integrated yields produced via converter method to give a hint of the performance of the whole assembly and of the potential of the method

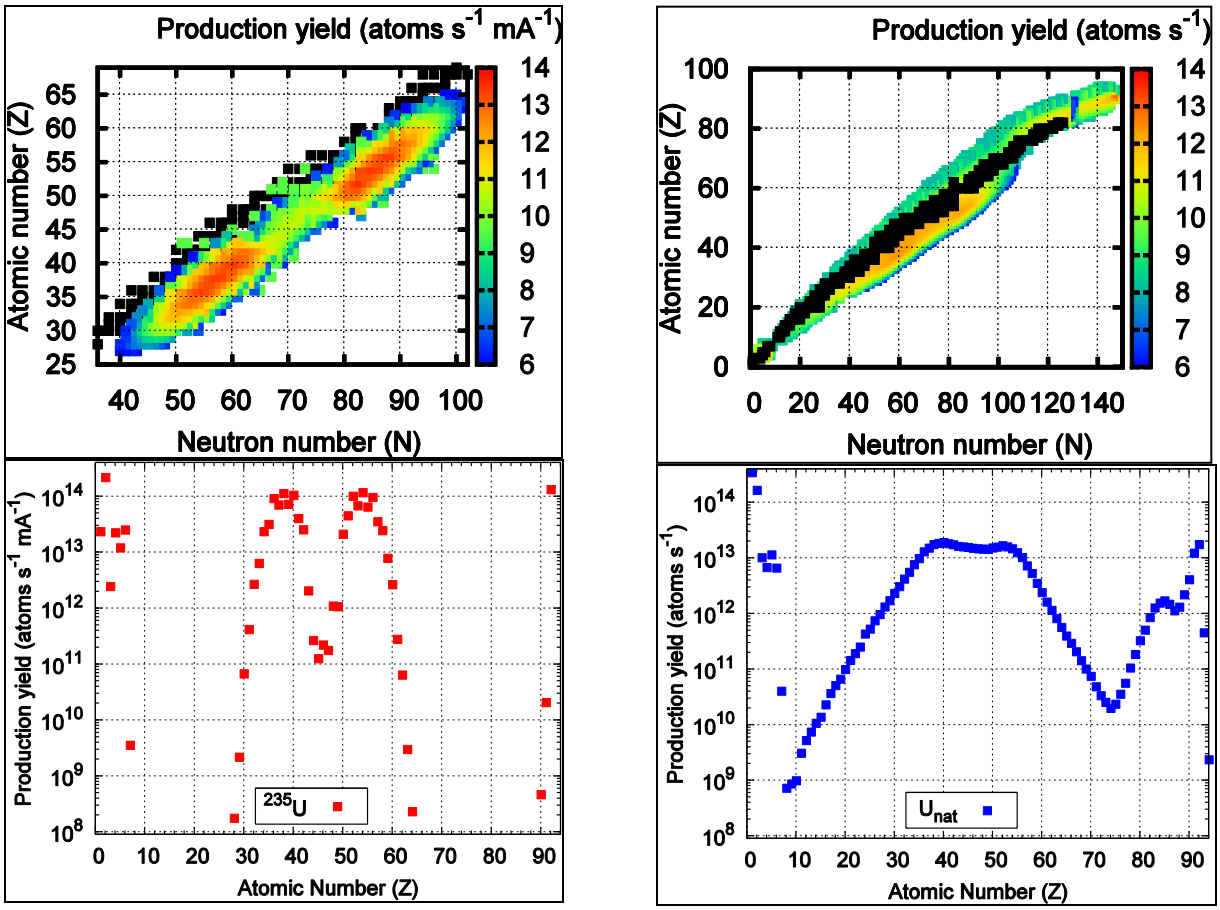

Figure 12: Comparison of the fission production rates. Top: in-target fission fragment distribution (stable isotopes are represented by black point); bottom: fission yields as a function of the atomic number (Z). Results of the converter method are shown on the left and of the direct method on the right

One can see that the isotopic distributions derived from the two analysed methods are very different: the high energy spallation provides a very broad production range, while the low energy fission gives the highest yields in the region covered by this process (30< Z <60).

The yields of neutron rich isotopes depend on the excitation energy which is taken by neutron emission before and after fission. In case of the converter method, the fission fragments which have large neutron excess will be weakly excited being therefore favourable for producing of the very rich neutron fission fragments. While the direct method is expected

to provide neutron-rich isotopes in a range extended largely outside low energy neutron induced fission region with quite high cross sections (Schmidt et al, 2007) and a certain number of neutron deficient nuclei (see Fig. 12).

Table 10: Comparison of the production yields for several relevant isotopes

	Direct (at. s^{-1})	**Converter** (at. s^{-1} mA^{-1})
^{91}Kr	1.3758 10^{12}	1.8154 10^{13}
^{93}Kr	3.7191 10^{11}	2.7748 10^{12}
^{80}Rb	2.2214 10^{10}	-
^{97}Rb	5.9786 10^{10}	2.2016 10^{11}
^{132}Sn	1.8294 10^{11}	3.3723 10^{12}
^{142}Xe	1.4876 10^{11}	2.5108 10^{12}
^{144}Xe	7.4205 10^{9}	3.4094 10^{10}
^{144}Cs	2.2806 10^{11}	2.4281 10^{12}
^{153}Sm	6.4680 10^{10}	4.6529 10^{8}
^{213}Fr	1.7372 10^{11}	

The Table 10 and Fig. 13 compare the two methods through the fission yields for selected relevant isotopes. As before integrated yields produced via converter method are used in comparison. The table clearly shows the advantage of the direct method in supplying high intensity spallation products (see ^{213}Fr) and neutron deficient nuclei (e.g. ^{80}Rb). This option is also more efficient in production of nuclides in vicinity of the main fission region; see the large difference (more than two orders of magnitudes) found for ^{153}Sm fission yields. On the other hand, the converter method gives appreciably higher in-target fission yields on the neutron-rich side when normalized to total number of fission events in the target.

This significant enhancement of the production yields is technically possible due to the deposition of the primary beam energy in the converter target.

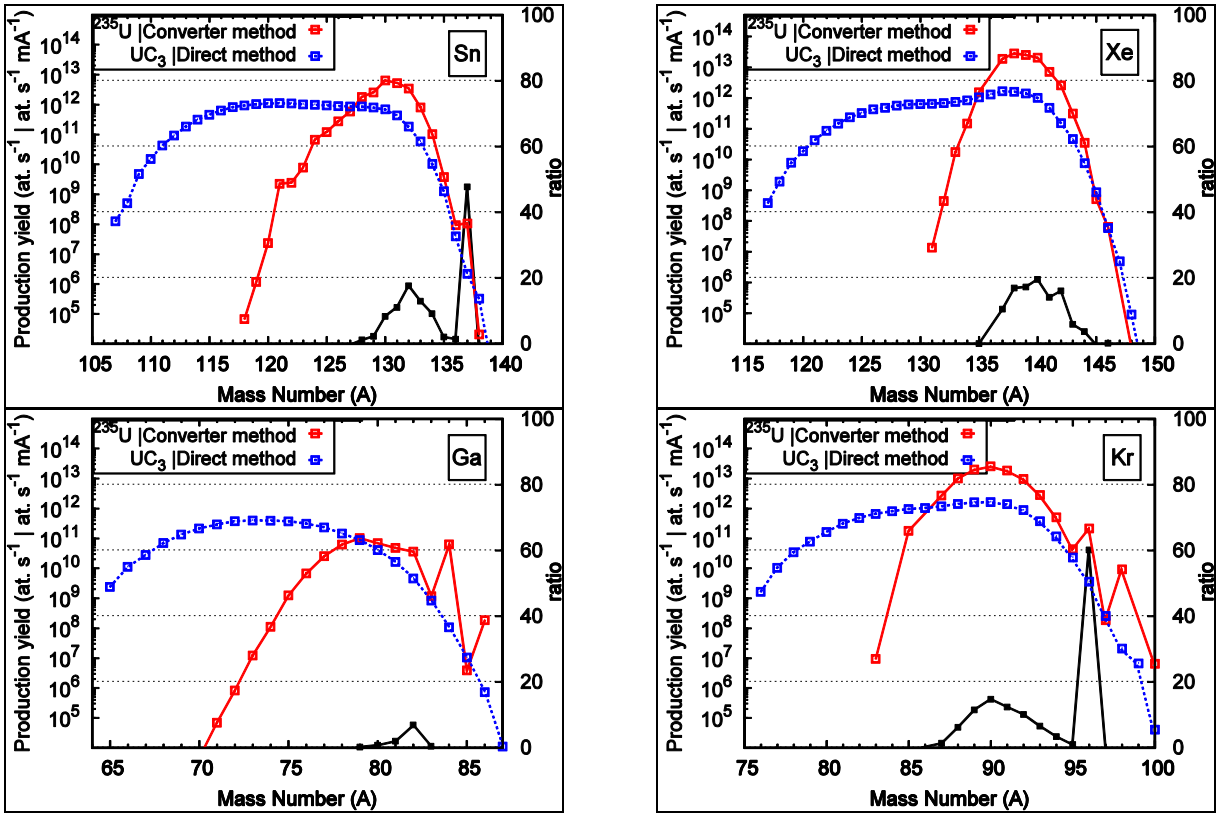

Figure 13: Comparison of the fission production yields by selected isotopes. Black curve is the ratio between converter and direct method results, scaled by the right y- axis. Only ratio values less than 100 are given in the graphs.

For the converter method the Fig. 13 reveals that high intensity production yields for heavy fission fragment group enhances with the number of neutrons inside the nuclide (see upper

panel of the Fig.) where the largest difference against the direct option reaches up to a factor 20 (for ^{140}Xe). Nuclides of the light fission fragment group are less favoured being less neutron rich (see Table 4 and Fig. 13, bottom).

One can conclude that the spallation of the optimized UC_3 target by 1 GeV protons and the fission induced by low energy secondary neutrons in a ^{235}U target are complementary methods able to provide overall high intensities for secondary beams over a large domain of the chart of the nuclides.

It is important to stress that the yields previously derived and analyzed are in-target products that have to leave the target in order to become useful. Therefore the reported values have to be corrected with the appropriate overall efficiencies, namely (release * delay * ion-source efficiency). For a rough judgement one can assume for the global extraction efficiencies the limits estimated for typical ISOLDE targets (Ravn, 1994) of ~ 10% for some isotopes with $T_{1/2}$ > 1 s and about ~ 1- 0.1% for $T_{1/2}$<1 s. However, release-time proprieties depend on both the element to be extracted and the target-ion-source characteristics requiring consequently more complex solutions. Quantitative estimates of the main features of the overall extraction efficiencies for a wide variety of isotope chains from different target and ion-source systems are provided in (Lukic et al, 2006).

Estimation of the intensity of secondary beams is beyond the scope of the present work.

4. Conclusions

A methodology has been developed to estimate the in-target fission yields arising from converter-fission targets assembly of the EURISOL facility. The last design variant of the converter target assembly received from the Task# 2 & 4 was used for this purpose. Calculation of the fission yields has been done using evaluated yields for the fission products tabulated at three energies of the neutron field. Integrated fission rates over three energy ranges have been therefore used as normalisation factors in order to derive the intensity of the total production yields. The procedure was also validated by applying an alternative method that uses CINDER to determine fission production rates. Based on this method the in-target fission yields were further derived and discussed for six isotopes of interest and six fission target configurations.

Calculations for the neutron flux have shown a quite uniform distribution over the six fission targets as well for all material configurations investigated. The neutron flux energy distribution is defined by neutron average kinetic energy of about 100 keV. This is optimum excitation energy for ^{236}U to produce neutron rich nuclei asymmetric distributed.

Due to the low neutron energies the fission process is induced essentially in ^{235}U. Consequently, for all accounted Uranium compounds more than half of the total fission rates are due to fission of the ^{235}U component. It was found that the number of fissions (~10^{15} per second) required by the baseline EURISOL project may be achieved for the most favourable producing system (^{235}U case). The use of other Uranium compounds or ^{232}Th is possible although it may reduce the magnitude of yields.

Detailed examination of the obtained fission products has been done with regard to the potential of the investigated target material configurations to enhance the production of specific nuclear species. In this respect ^{235}U based fission targets supply maximum intensity production yields for nuclides like: ^{92}Kr (6.6 10^{12} at. s^{-1} mA^{-1}), ^{132}Sn (3.4 10^{12} at. s^{-1} mA^{-1}), ^{142}Xe (2.5 10^{12} at. s^{-1} mA^{-1}), but one expect that the maximum in-target yield for ^{126}Ag (of 10^{8} at. s^{-1} mA^{-1}) or ^{80}Ni (10^{2} at. s^{-1} mA^{-1}) to be produced by ^{232}Th material.

Comparison of the ^{235}U production rates with the SPIRAL2 similar estimates (for 10^{14} fiss s^{-1}) had proven the net profit given by the EURISOL compact 4-MW target design in obtaining high intensity fission yields (up to two order of magnitude differences).

A comparative study between the two production scenarios used in the design, converter and direct methods, in terms of the relevant fission product yields was finally carried-out for actinide based targets. The obtained results validate quantitatively the benefits of each of the method used. The converter system provides the highest fission yields defined by the 10^{15} fiss s^{-1} for a limited number of nuclides while an actinide direct target in addition might produce a broad range (spallation, fission, fragmentation regions) of other isotopes of interests at intensities higher than of those of the existing facilities.

The quantitative estimates of the fission production rates obtained in this study together with the analysis of the complementary advantages of the two production methods used in the design allow to have a picture of the figure of merit of the designed installation.

The obtained results have to be corrected with the appropriate overall efficiencies in order to get the secondary beam intensity predictions at the future EURISOL facility.

Acknowledgements

We acknowledge the financial support of the EC under the FP6 "Research Infrastructure Action - Structuring the European Research Area "EURISOL DS Project; Contract No. 515768 RIDS; www.eurisol.org. The EC is not liable for any use that may be made of the information contained herein.

5. References

EURISOL design study: <http://www.eurisol.org>

<http://www.nndc.bnl.gov>

Chabod, S., et al. Optimization of in-target yields for RIB production. Part I: direct targets. IR:IRFU-08-21, (2008) on www.eurisol.org

Cornell, J., (Ed.). EURISOL report –Appendix C. Targets and Ion sources for EURISOL. Ganil. December 2003. http://www.ganil.fr/eurisol/Final_Report.html

England, T., R. and Rider, B., F., ENDF-349 Evaluation and Compilation of Fission Product Yields. LA-UR-94-31106. 1994. data from http://ie.lbl.gov/fission.html

Fadil, M., Rannou, B. About the production rates and the activation of the uranium carbide target for SPIRAL 2, NIMB, Vol. 266, 19-20, 4318(2008)

Herrera-Martinez, A. et al. EURISOL Multi-MW Target Neutron Flux and fission rate calculations for MAFF configuration (2007). work report available on www.eurisol.org

Lukic, S., et al. Systematic comparison of ISOLDE-SC yields with calculated in-target production rates. NIMA 565. pp 784. (2006)

Hendricks, J. et al., MCNPX user manual. version 2.5.0, LA-UR-05-2675, 2005

Prael. R.E., Lichtenstein H., User Guide to LCS : The Lahet Code System. Report No. LA-UR-89-3014. Los Alamos National Laboratory. September (1989)

Ravn, H., L. et al., Comparison of radioactive ion-beam intensities produced by means of thick targets bombarded with neutrons, protons and heavy ions, NIMB 88 (1994), 441

Romanets, Y., private communication (2009)

Schmidt, K.H. et al. Studies on the benefit of extended capability of the driver accelerator for EURISOL, Phys Rev Special Topics –Accelerators and Beams 10, 014701, (2007)

Wilson, W. B. and England, T., R., A manual for CINDER.90 version C00D and associated codes and data. LA-UR-00-Draft (2001)

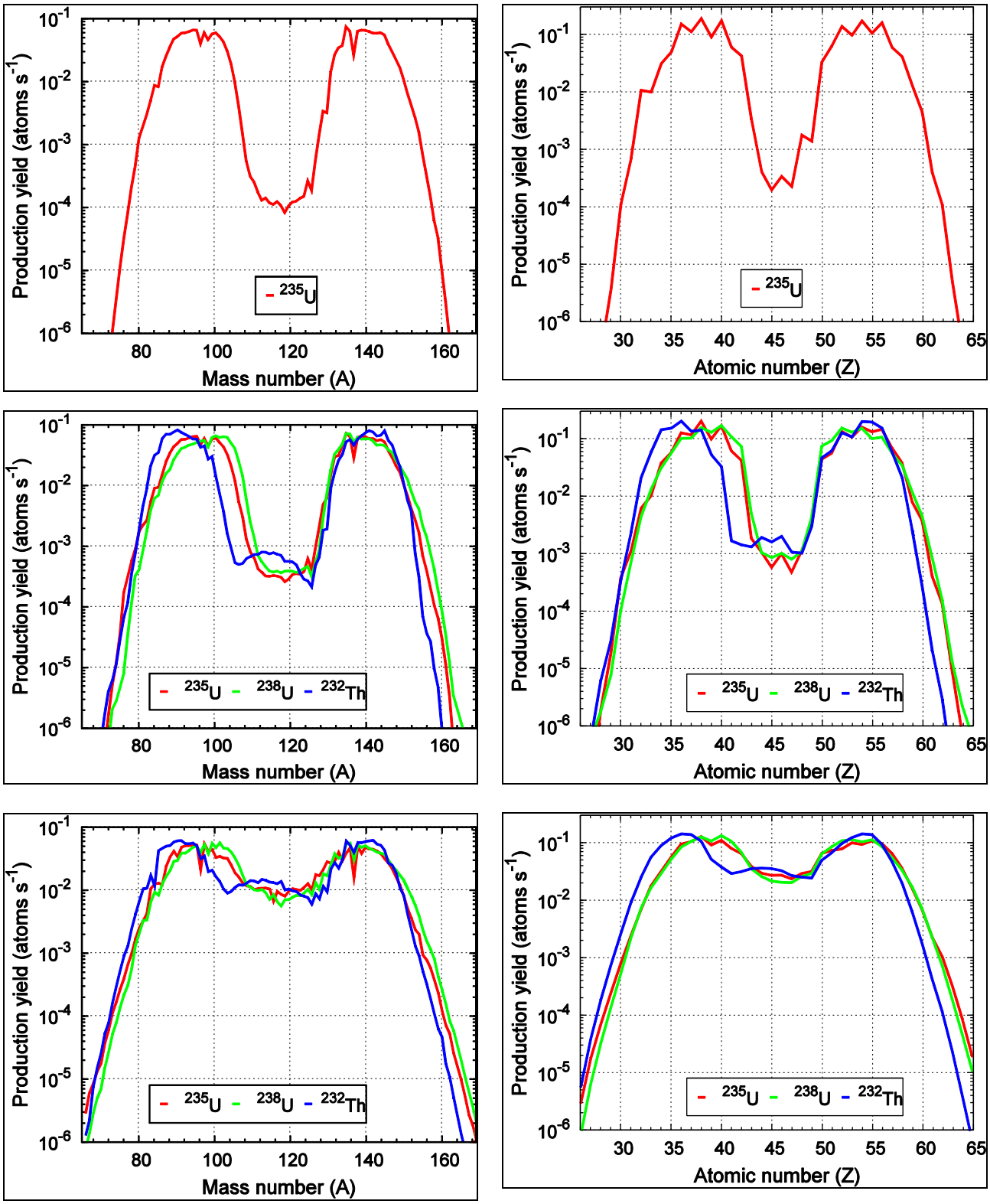

FigureA1.1: Tabulated fission yields as a function of the mass number (A) on the left and on atomic number (Z) on the right. From top to bottom: Therm, Fast and High Energy

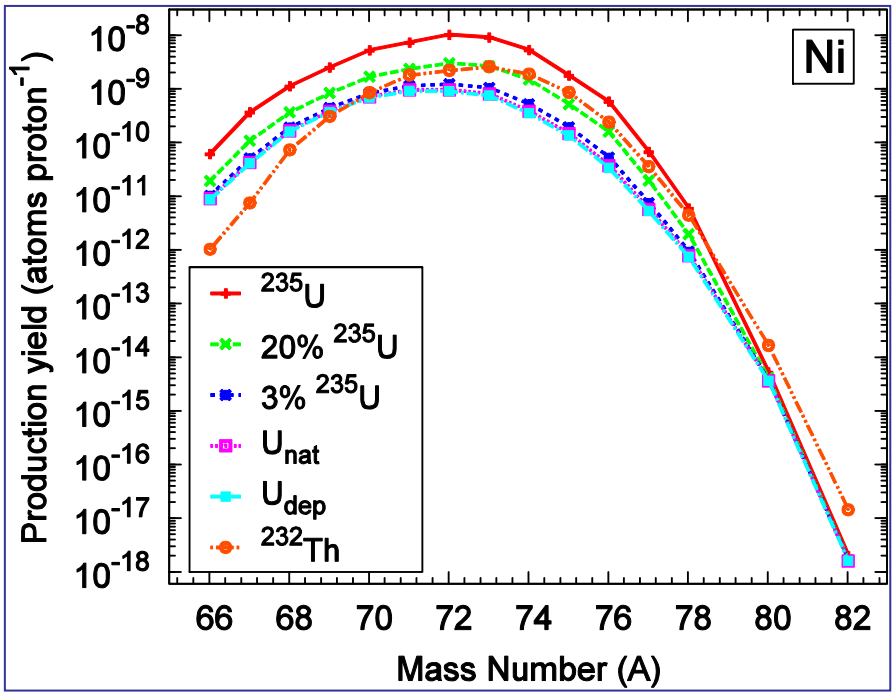

Figure A1.1 In-target production rates for **Ni**

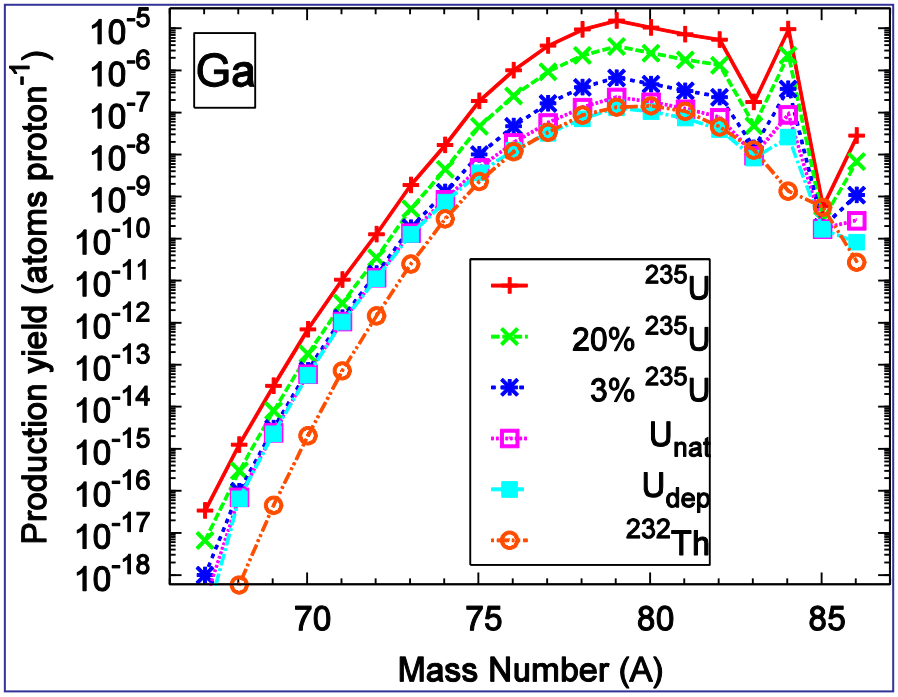

Figure A1.2 In-target production rates for **Ga**

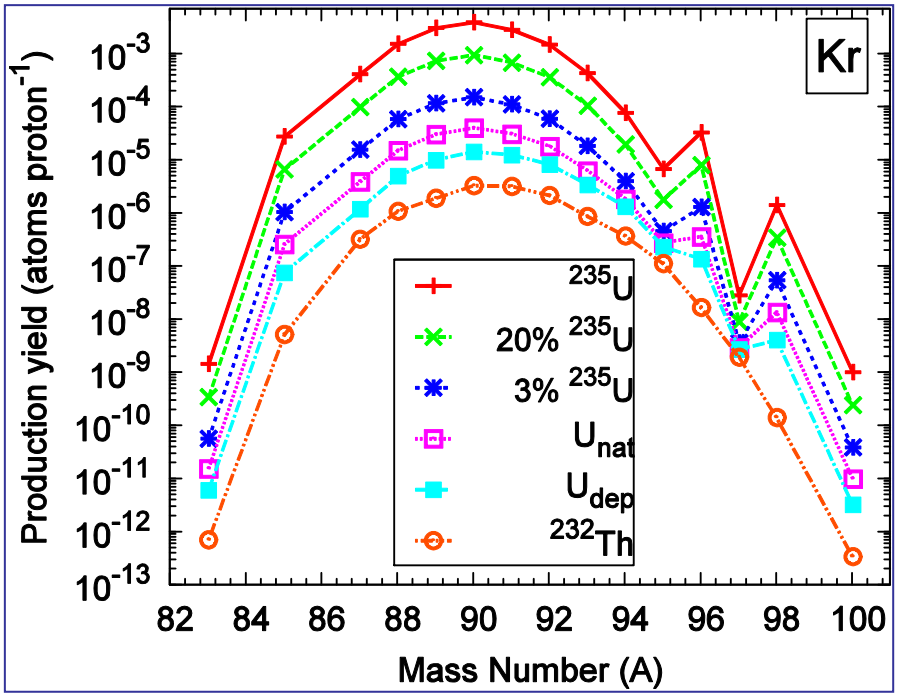

Figure A1.3 In-target production rates for **Kr**

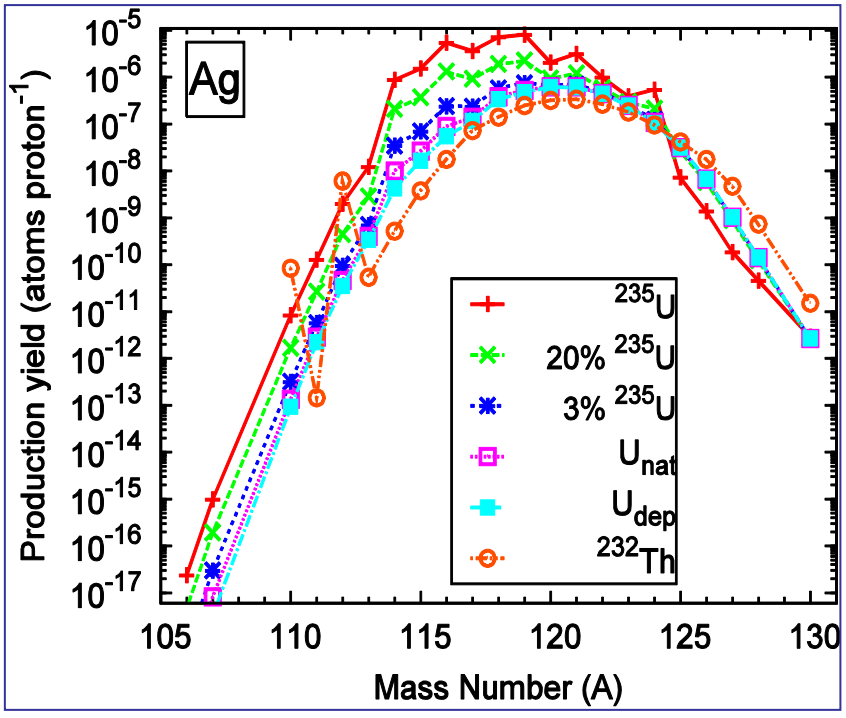

Figure A1.4 In-target production rates for **Ag**

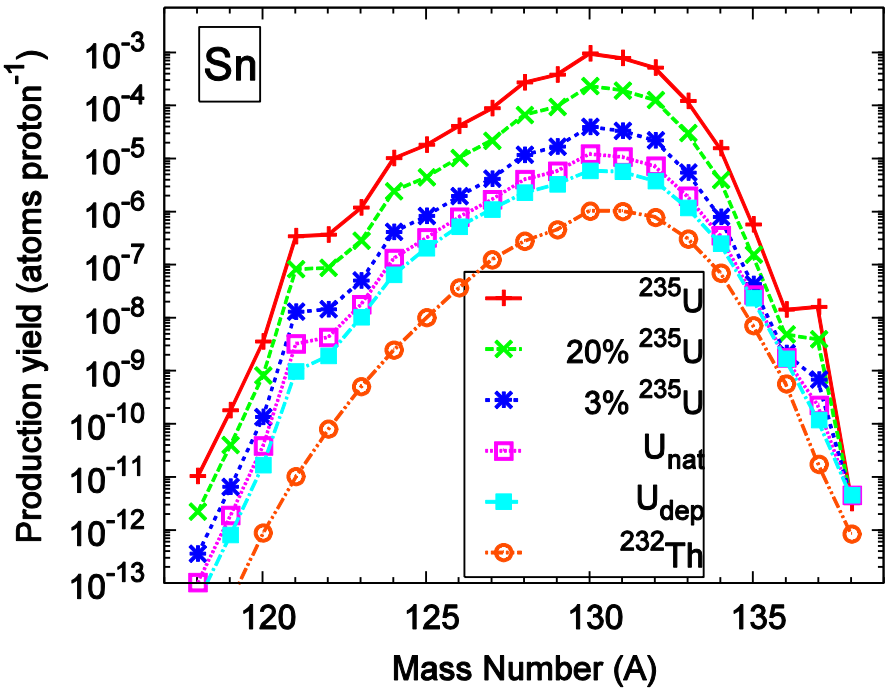

Figure A1.5 In-target production rates for **Sn**

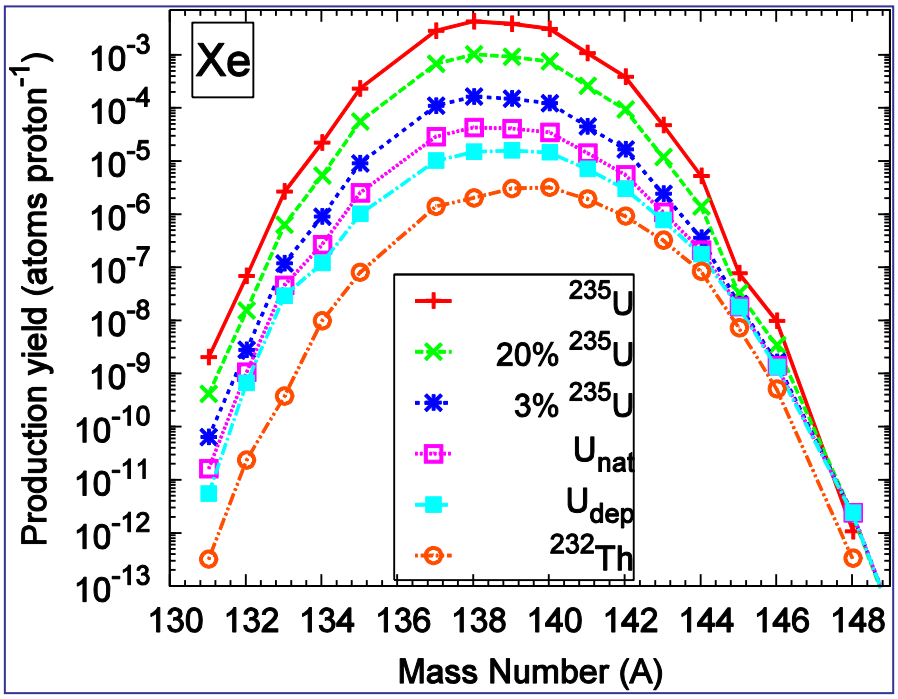

Figure A1.6 In-target production rates for **Xe**

Annexe 2

Table A2.1: In-target production rates for Ni [atoms s-1 mA-1]

A	$T_{1/2}$	100% ^{235}U	20% ^{235}U	3% ^{235}U	U_{nat}	U_{dep}	^{232}Th
66	54.6 h	6.2856E-11	1.9776E-11	1.0529E-11	9.2863E-12	8.9942E-12	1.0578E-12
67	21 s	3.7651E-10	1.1123E-10	5.2141E-11	4.4121E-11	4.2250E-11	7.7823E-12
68	19 s	1.1615E-09	3.7823E-10	1.9663E-10	1.7178E-10	1.6594E-10	7.5681E-11
69	10 s	2.5814E-09	8.6056E-10	4.5293E-10	3.9688E-10	3.8370E-10	3.1899E-10
70		5.3558E-09	1.7308E-09	8.5653E-10	7.3578E-10	7.0748E-10	8.8289E-10
71		7.5574E-09	2.4186E-09	1.1639E-09	9.9019E-10	9.4948E-10	1.8762E-09
72	3.83 s	1.0538E-08	3.1138E-09	1.2557E-09	9.9683E-10	9.3657E-10	2.2774E-09
73	0.491 s	9.3488E-09	2.7360E-09	1.0657E-09	8.3243E-10	7.7822E-10	2.6825E-09
74	0.900 s	5.4735E-09	1.5417E-09	5.3564E-10	3.9472E-10	3.6205E-10	1.9627E-09
75	0.231 s	1.8427E-09	5.3357E-10	1.9813E-10	1.5114E-10	1.4022E-10	8.9116E-10
76	0.305 s	5.9771E-10	1.6454E-10	5.4077E-11	3.8614E-11	3.5034E-11	2.4721E-10
77	0.103 s	6.9261E-11	2.0202E-11	7.6531E-12	5.8958E-12	5.4881E-12	3.6958E-11
78	0.132 s	6.0821E-12	2.0189E-12	9.5300E-13	8.0312E-13	7.6822E-13	4.5857E-12
80		5.3598E-15	4.2059E-15	3.8144E-15	3.7587E-15	3.7431E-15	1.7248E-14
82		2.0372E-18	1.7448E-18	1.6574E-18	1.6458E-18	1.6415E-18	1.4927E-17

Annexe 2

Table A2.2: In-target production rates for Ga

A	$T_{1/2}$	100% ^{235}U	20% ^{235}U	3% ^{235}U	Nat.U	Depl.U	^{232}Th
67	3.261 d	3.5751E-17	6.9579E-18	1.0391E-18	2.4920E-19	6.9147E-20	
68	68.06 m	1.3262E-15	3.1193E-16	1.0235E-16	7.4379E-17	6.7941E-17	6.0637E-19
69	stable	3.3374E-14	8.4027E-15	3.2310E-15	2.5408E-15	2.3812E-15	4.7685E-17
70	21.1 m	7.2933E-13	1.8978E-13	7.7289E-14	6.2257E-14	5.8774E-14	2.1568E-15
71	stable	1.1085E-11	3.0670E-12	1.3618E-12	1.1330E-12	1.0798E-12	7.5568E-14
72	14.10 h	1.3211E-10	3.6703E-11	1.5286E-11	1.2372E-11	1.1695E-11	1.5244E-12
73	4.87 h	1.9609E-09	5.3665E-10	1.9109E-10	1.4321E-10	1.3210E-10	2.6192E-11
74	8.1 m	1.7677E-08	4.6474E-09	1.3441E-09	8.8196E-10	7.7516E-10	3.0858E-10
75	2.10 m	1.9724E-07	4.9139E-08	1.0534E-08	5.1002E-09	3.8485E-09	2.3949E-09
76	29 s	1.0698E-06	2.6019E-07	4.9685E-08	2.0068E-08	1.3254E-08	1.2225E-08
77	13.0 s	4.0627E-06	9.7806E-07	1.7282E-07	5.9428E-08	3.3352E-08	3.5387E-08
78	5.09 s	9.8835E-06	2.3902E-06	4.1618E-07	1.3768E-07	7.3635E-08	9.0809E-08
79	2.85 s	1.6136E-05	3.9290E-06	6.9793E-07	2.4163E-07	1.3668E-07	1.4087E-07
80	1.68 s	1.1030E-05	2.7010E-06	4.9455E-07	1.8290E-07	1.1121E-07	1.5103E-07
81	1.22 s	7.6023E-06	1.8676E-06	3.4235E-07	1.2676E-07	7.7167E-08	1.1174E-07
82	0.607 s	5.7090E-06	1.3941E-06	2.4184E-07	7.8830E-08	4.1341E-08	4.7525E-08
83	0.31 s	1.8624E-07	5.1197E-08	1.5031E-08	9.9144E-09	8.7364E-09	1.3439E-08
84	0.098 s	1.0019E-05	2.4134E-06	3.8090E-07	9.3284E-08	2.7154E-08	1.4130E-09
85	0.087 s	6.2050E-10	2.9324E-10	1.9346E-10	1.7907E-10	1.7573E-10	5.8232E-10
86		2.9605E-08	7.1367E-09	1.1317E-09	2.8196E-10	8.6565E-11	2.8815E-11

Table A2.3: In-target production rates for Kr

A	$T_{1/2}$	100% ^{235}U	20% ^{235}U	3% ^{235}U	Nat.U	Depl.U	^{232}Th
83-m	1.83 h	1.4877E-09	3.5602E-10	5.7946E-11	1.5887E-11	6.2176E-12	7.2560E-13
85-m	4.48 h	5.3343E-06	1.2838E-06	2.0230E-07	4.9292E-08	1.4113E-08	6.0244E-10
85	10.73y	2.3126E-05	5.5656E-06	8.7863E-07	2.1557E-07	6.3113E-08	4.7103E-09
87	1.27 h	4.2581E-04	1.0223E-04	1.6179E-05	4.0152E-06	1.2186E-06	3.3154E-07
88	2.84 h	1.5871E-03	3.8169E-04	6.0884E-05	1.5528E-05	5.0997E-06	1.1118E-06
89	3.15 m	3.1566E-03	7.5916E-04	1.2119E-04	3.0990E-05	1.0251E-05	1.9586E-06
90	32.3 s	4.0505E-03	9.7465E-04	1.5671E-04	4.1081E-05	1.4498E-05	3.3792E-06
91	8.6 s	2.9093E-03	7.0194E-04	1.1475E-04	3.1730E-05	1.2645E-05	3.2718E-06
92	1.84 s	1.5248E-03	3.6957E-04	6.1880E-05	1.8374E-05	8.3711E-06	2.2189E-06
93	1.29 s	4.4468E-04	1.0874E-04	1.9075E-05	6.3895E-06	3.4729E-06	8.8879E-07
94	0.21 s	7.9631E-05	2.0095E-05	4.1378E-06	1.8789E-06	1.3595E-06	3.7951E-07
95	0.78 s	6.9310E-06	1.8330E-06	4.7330E-07	2.8107E-07	2.3687E-07	1.1538E-07
96	0.293s	3.4160E-05	8.2671E-06	1.3448E-06	3.6522E-07	1.3999E-07	1.7198E-08
97	0.1 s	2.9148E-08	9.1744E-09	3.7388E-09	2.9684E-09	2.7898E-09	1.9889E-09
98	0.160 s	1.4712E-06	3.5454E-07	5.6099E-08	1.3870E-08	4.1594E-09	1.4499E-10
100		1.0379E-09	2.5044E-10	3.9949E-11	1.0163E-11	3.3135E-12	3.5028E-13

Table A2.4: In-target production rates for Ag

A	$T_{1/2}$	100% ^{235}U	20% ^{235}U	3% ^{235}U	Nat.U	Depl.U	^{232}Th
106	8.4 d	2.3568E-17	4.5867E-18	6.8502E-19	1.6428E-19	4.5583E-20	
107-m	44 s	9.0076E-16	1.7531E-16	2.6181E-17	6.2788E-18	1.7422E-18	
107	stable	7.8293E-17	1.6406E-17	3.6615E-18	1.9606E-18	1.5715E-18	
110-m	252 d	8.2709E-12	1.6726E-12	3.1483E-13	1.3363E-13	9.2247E-14	8.3595E-11
111-m	1.08 m	1.1822E-10	2.4518E-11	5.1908E-12	2.6103E-12	2.0202E-12	1.3248E-13
111	7.47 d	1.0323E-11	2.1418E-12	4.5211E-13	2.2644E-13	1.7483E-13	1.1541E-14
112	3.13 h	1.9773E-09	4.4450E-10	9.3888E-11	4.5876E-11	3.4860E-11	6.0637E-09
113-m	1.14 m	1.1023E-08	2.5324E-09	6.3003E-10	3.7084E-10	3.1129E-10	4.9380E-11
113	5.3 h	1.1687E-09	2.7049E-10	6.2617E-11	3.4080E-11	2.7523E-11	4.3022E-12
114	4.6 s	8.6834E-07	2.0882E-07	3.4476E-08	9.8587E-09	4.1979E-09	5.1731E-10
115-m	18.7 s	1.2891E-06	3.1310E-07	5.4528E-08	1.8002E-08	9.5993E-09	1.8697E-09
115	20 m	2.2681E-07	5.7370E-08	1.4315E-08	8.2867E-09	6.8964E-09	1.8697E-09
116-m	10.5 s	8.9385E-07	2.2244E-07	5.1882E-08	2.7999E-08	2.2497E-08	8.7529E-09
116	2.68 m	4.4814E-06	1.0861E-06	1.8769E-07	6.0810E-08	3.1625E-08	8.7529E-09
117-m	5.3 s	1.8196E-06	4.6121E-07	1.1731E-07	6.9204E-08	5.8108E-08	3.6310E-08
117	1.22 m	1.8196E-06	4.6121E-07	1.1731E-07	6.9204E-08	5.8108E-08	3.6310E-08
118-m	2.4 s	3.3736E-06	9.1162E-07	2.7704E-07	1.8799E-07	1.6738E-07	6.9680E-08
118	4.0 s	3.7617E-06	1.0050E-06	2.9173E-07	1.9154E-07	1.6837E-07	6.9680E-08
119	2.1s	8.1220E-06	2.2579E-06	7.3947E-07	5.2622E-07	4.7682E-07	2.4805E-07
120	1.23 s	2.0439E-06	9.3217E-07	6.5638E-07	6.1832E-07	6.0902E-07	3.1802E-07
121	0.78 s	3.1184E-06	1.2055E-06	6.9289E-07	6.2069E-07	6.0353E-07	3.3656E-07
122	0.56 s	9.8860E-07	5.7972E-07	4.5978E-07	4.4279E-07	4.3846E-07	2.6501E-07
123	0.31 s	3.8799E-07	2.8870E-07	2.5239E-07	2.4715E-07	2.4570E-07	1.8008E-07
124	0.22 s	5.3661E-07	2.1267E-07	1.2099E-07	1.0793E-07	1.0483E-07	9.5454E-08
125	0.334 s	7.2117E-09	2.7258E-08	3.0847E-08	3.1326E-08	3.1405E-08	4.1397E-08
126	0.140 s	1.3705E-09	5.7864E-09	6.5824E-09	6.6889E-09	6.7066E-09	1.7602E-08
127	0.175 s	1.8609E-10	8.8418E-10	1.0105E-09	1.0274E-09	1.0303E-09	4.6861E-09
128	0.094 s	4.5547E-11	1.2474E-10	1.3866E-10	1.4054E-10	1.4082E-10	7.3000E-10
130		2.8729E-12	2.7141E-12	2.6525E-12	2.6452E-12	2.6408E-12	1.4894E-11

Table A2.5: In-target production rates for Sn

A	$T_{1/2}$	100% ^{235}U	20% ^{235}U	3% ^{235}U	Nat.U	Depl.U	^{232}Th
118	stable	1.0780E-11	2.2875E-12	3.6895E-13	1.0688E-13	4.6914E-14	2.2018E-15
119-m	293 d	1.8737E-10	4.1530E-11	6.7525E-12	1.9446E-12	8.4251E-13	4.9770E-14
120	stable	3.7188E-09	8.5469E-10	1.3993E-10	4.0166E-11	1.7264E-11	9.0862E-13
121-m	55 y	3.1519E-08	7.3629E-09	1.2252E-09	3.6536E-10	1.6786E-10	8.6156E-12
121	1.128d	3.2469E-07	7.8109E-08	1.2296E-08	2.9863E-09	8.4557E-10	1.9389E-12
122	stable	3.8297E-07	9.0487E-08	1.5032E-08	4.4290E-09	1.9927E-09	8.2481E-11
123-m	40.1 m	3.2969E-07	7.8101E-08	1.3400E-08	4.3155E-09	2.2278E-09	9.8893E-11
123	129.2d	9.0939E-07	2.1524E-07	3.8859E-08	1.4154E-08	8.4765E-09	4.2390E-10
124	stable	1.0538E-05	2.5278E-06	4.3087E-07	1.3537E-07	6.7426E-08	2.5483E-09
125-m	9.5 m	9.7799E-06	2.3647E-06	3.9706E-07	1.1902E-07	5.5075E-08	2.0217E-09
125	9.63 d	9.1182E-06	2.2389E-06	4.6368E-07	2.1427E-07	1.5688E-07	8.4148E-09
126	1.e5y	4.3275E-05	1.0627E-05	2.0336E-06	8.2164E-07	5.4268E-07	3.7862E-08
127-m	4.15 m	8.7378E-06	2.1623E-06	4.7862E-07	2.4253E-07	1.8817E-07	2.4242E-08
127	2.12 h	8.3544E-05	2.0469E-05	3.8426E-06	1.4968E-06	9.5699E-07	1.0397E-07
128	59.1 m	2.8280E-04	6.8890E-05	1.2209E-05	4.2025E-06	2.3608E-06	2.8601E-07
129-m	6.9 m	1.8094E-04	4.3773E-05	7.2950E-06	2.1385E-06	9.5294E-07	8.6644E-08
129	2.4 m	2.2008E-04	5.3934E-05	1.0055E-05	3.8620E-06	2.4376E-06	3.8491E-07
130	3.7 m	1.0008E-03	2.4265E-04	4.1154E-05	1.2676E-05	6.1282E-06	1.0578E-06
131	39 s	8.2159E-04	1.9965E-04	3.4543E-05	1.1212E-05	5.8483E-06	1.0444E-06
132	40 s	5.4043E-04	1.3199E-04	2.2905E-05	7.4730E-06	3.9251E-06	8.0049E-07
133	1.44 s	1.2714E-04	3.1241E-05	5.6624E-06	2.0444E-06	1.2129E-06	3.1587E-07
134	1.04 s	1.6286E-05	4.0937E-06	8.2815E-07	3.6592E-07	2.5971E-07	7.2074E-08
135	0.418s	5.9621E-07	1.6161E-07	4.4587E-08	2.8009E-08	2.4205E-08	7.3389E-09
136	0.717s	1.4788E-08	5.0077E-09	2.2355E-09	1.8392E-09	1.7485E-09	5.8530E-10
137		1.6794E-08	4.1114E-09	7.1378E-10	2.3281E-10	1.2223E-10	1.7889E-11
138		3.3149E-12	4.7234E-12	4.6840E-12	4.6689E-12	4.6641E-12	8.6635E-13

Table A2.6: In-target production rates for Xe

A	$T_{1/2}$	100% ^{235}U	20% ^{235}U	3% ^{235}U	Nat.U	Depl.U	^{232}Th
131-m	11.9 d	2.1341E-09	4.3094E-10	6.6148E-11	1.6950E-11	5.7165E-12	3.3396E-13
132	stable	7.0957E-08	1.6003E-08	2.9156E-09	1.1068E-09	6.9190E-10	2.4411E-11
133-m	2.19 d	2.0677E-06	4.9689E-07	9.4177E-08	3.7667E-08	2.4671E-08	3.2071E-10
133	5.243d	6.8823E-07	1.6495E-07	2.9299E-08	1.0221E-08	5.8349E-09	7.0835E-11
134-m	0.29 s	2.3238E-05	5.6004E-06	9.3533E-07	2.7659E-07	1.2510E-07	1.0218E-08
135-m	15.3 m	1.6608E-04	3.9939E-05	6.5029E-06	1.7792E-06	6.9306E-07	6.8992E-08
135	9.10 h	7.3975E-05	1.7803E-05	2.9473E-06	8.4977E-07	3.6744E-07	1.4966E-08
137	3.82 m	2.9497E-03	7.0921E-04	1.1411E-04	3.0005E-05	1.0669E-05	1.4548E-06
138	14.1 m	4.4330E-03	1.0662E-03	1.7122E-04	4.4701E-05	1.5614E-05	2.1018E-06
139	39.7 s	3.9728E-03	9.5815E-04	1.5603E-04	4.2631E-05	1.6559E-05	3.1649E-06
140	13.6 s	3.2176E-03	7.7810E-04	1.2826E-04	3.6371E-05	1.5244E-05	3.3233E-06
141	1.72 s	1.1179E-03	2.7221E-04	4.6680E-05	1.4782E-05	7.4490E-06	2.0273E-06
142	1.22 s	4.0237E-04	9.8156E-05	1.7226E-05	5.7857E-06	3.1559E-06	9.6326E-07
143	0.30 s	4.9046E-05	1.2331E-05	2.5168E-06	1.1283E-06	8.0908E-07	3.3822E-07
144	1.2 s	5.4638E-06	1.4614E-06	3.7385E-07	2.1951E-07	1.8404E-07	8.7089E-08
145	0.9 s	8.0659E-08	3.4398E-08	2.0972E-08	1.9048E-08	1.8608E-08	7.5646E-09